Modelling of the mechanical behavior of a copper-base alloy using Chaboche model´s constitutive equations

Wissam Bouajila and Jörg Riccius**
** Deutsches Zentrum für Luft- und Raumfahrt (DLR) – Lampoldshausen, Institute of Space Propulsion*
Im Langen Grund, D-74239 Hardthausen, Germany

Abstract

A step-by-step procedure for the identification of the Chaboche model´s parameters applied to a copper-base alloy that may be considered as a cost efficient material for a rocket engine combustion chamber inner liner is presented in this paper. Experimental data from a strain-controlled uniaxial low cycle fatigue test and a stress relaxation test are used for the identification of the model´s parameters. In addition to the fatigue test and the stress relaxation test, a dwell test with a hold period of 600 s at extreme strain amplitude in tension and compression is considered for the assessment of the accuracy of the identified model parameters. The comparisons of the predictions of the model with optimized parameters to the above mentioned experiments at 900 K for the considered copper-based alloy are presented.

1 Introduction

The strong demand for light-weight structures for space transportation systems leads to a close-to-the-limit design of the components – including the rocket engine. The inner liner of a regeneratively cooled wall of a main stage rocket combustion chamber is extremely loaded by the high temperature of the hot gas and the pressure difference between the coolant and the hot gas. An understanding of the material behaviour at such conditions is very important for the fatigue life prediction of the structure.

Among the several viscoplasticity constitutive models proposed for predicting material behaviors at high temperatures, the unified Chaboche viscoplasticity model has been widely accepted. The unified Chaboche constitutive model has received much attention due to its simplicity to comprehend and use. The Chaboche model is capable of simulating cyclic plasticity, strong deformation rate effects, and other time dependent processes such as creep, stress relaxation and static/dynamic recovery.

Although the Chaboche model is widely used, few references in literature [1] [2] provide detailed information on whose tests have to be carried out and how one has to process the experimental data to determine a complete set of material parameters to be used within the model.

The purpose of the present paper is to provide the reader with an as detailed as possible guideline on the identification of the unified Chaboche model using uniaxial tests data. A step by step procedure in the characterization of the model parameters is suggested.

A copper base alloy that may be used as a cost efficient material for a rocket engine combustion chamber inner liner is considered for this work. Experimental data from a strain-controlled uniaxial low cycle fatigue and from a uniaxial stress relaxation test are used to illustrate the material parameter identification procedure.

In addition to the fatigue test and the stress relaxation test, a strain-controlled uniaxial dwell test with holding periods in tension and compression is considered for the assessment of the accuracy of the identified model parameters. The comparison of the predictions of the model with the optimized parameters to the data from the above mentioned tests at 900 K are presented in this paper.

2 Material model

2.1 Constitutive equations of the unified Chaboche model

The decomposition of the total strain $\boldsymbol{\varepsilon}$ can be assumed as

$$\boldsymbol{\varepsilon} = \boldsymbol{\varepsilon}_e + \boldsymbol{\varepsilon}_{th} + \boldsymbol{\varepsilon}_p \tag{1}$$

with $\boldsymbol{\varepsilon}_e$ the elastic strain, $\boldsymbol{\varepsilon}_{th}$ the thermal strain , and $\boldsymbol{\varepsilon}_p$ the inelastic strain except the thermal strain.

At a constant temperature and within the uniaxial small-strain hypothesis, the resulting stress increment $\dot{\sigma}$ is given in equation (2) according to Hook´s law for an isotropic elastic material:

$$\dot{\sigma} = E\left(\dot{\varepsilon} - \dot{\varepsilon_p}\right) \tag{2}$$

with E the Young´s modulus of the material.

The uniaxial form of the Chaboche model as described in [3] is adopted in the present paper. The basic equation is the flow rule, which determines the evolution of the inelastic strain as a function of the external stress σ and internal variables such as the back stress χ and the drag stress R:

$$\dot{\varepsilon}_p = \langle\frac{f}{Z}\rangle^n \operatorname{sgn}(\sigma - \chi) \tag{3}$$

where the McCauley brackets $\langle\cdot\rangle$ are here defined as

$$\langle x\rangle = \begin{cases} x, & x > 0, \\ 0, & x \leq 0. \end{cases} \tag{4}$$

and where the sign function *sgn* is defined as

$$\operatorname{sgn}(x) = \begin{cases} 1, & x > 0, \\ 0, & x = 0, \\ -1, & x < 0, \end{cases} \tag{5}$$

The yield criterion is given by

$$f = J(\sigma - \chi) - R - k \tag{6}$$

where k corresponds to the initial size of the yield surface and is referring to the true elastic limit of the material and J determines the scalar equivalent of the deviatoric stress state:

$$J(\sigma - \chi) = |\sigma - \chi| \tag{7}$$

The elastic domain is defined by $f \leq 0$ and the inelastic domain by $f > 0$.

2.2 Hardening terms

2.2.1 Kinematic hardening

The kinematic hardening χ is used to capture directional dependent effects such as the Bauschinger effect due to the plastic flow under cyclic loading. In a three dimensional principal stress space, it corresponds to a translation of the elastic domain. It may have multiple terms as follows:

$$\chi = \sum_{i=1}^{M} \chi_i \tag{8}$$

The evolution equation of the back stress χ for non-linear kinematic hardening used in the Chaboche model was originally introduced by Armstrong and Frederik [4]

$$\dot{\chi}_i = C_i \dot{\varepsilon_p} - \gamma_i \chi_i \dot{p} \tag{9}$$

where p is the accumulated plastic strain and defined as

$$\dot{p} = \left|\dot{\varepsilon}_p\right| \tag{10}$$

The stationary values of χ_i are given by C_i/γ_i while the values of γ_i indicate the speed with which the stationary values are reached. For linear kinematic hardening, $\gamma_i = 0$. Residual stresses may be taken into account by taking non-zero initial values χ_i^0, where its values may depend on the loading history.

2.2.2 Isotropic hardening

The isotropic hardening R is used to describe directionally independent effects such as the change in the size of the yield surface during cyclic loading as for the cyclic hardening or for the cyclic softening. In a three dimensional principal stress space, it corresponds to an expansion or a contraction of the elastic domain around its origin. As for the kinematic hardening, it may have multiple terms as follows:

$$R = \sum_{j=1}^{N} R_j \tag{11}$$

The evolution of R_j follows the accumulated plastic strain p. The evolution equation of R_j for a non-linear isotropic hardening is defined as

$$\dot{R}_j = b_j\left(Q_j - R_j\right)\dot{p} \tag{12}$$

where Q_j is the stationary value of R_j while b_j indicates the speed with which the stationary value is reached.

For linear isotropic hardening, the evolution equation of R_j is

$$\dot{R}_j = R_{0,j}\dot{p} \tag{13}$$

with $R_{0,j}$ is the asymptotic value of the isotropic hardening R_j.

2.3 Viscous behaviour

A viscous overstress function is considered to describe the rate dependency of the stress. The rate dependency of the stress and therefore the creep effect is accounted for within the model in the form of the Norton creep law [5] as follows

$$\sigma_v = Z\dot{p}^{1/n} \tag{14}$$

where, σ_v is the viscous stress and Z and n are the viscous parameters.

At each moment the stress is given by

$$\sigma = \chi + \nu(R + k + \sigma_v) \tag{15}$$

where $\nu = \text{sgn}(\sigma - \chi) = \pm 1$ according to the direction of the flow.

2.4 Model´s parameters

From this model description, the parameters shown in **Table 1** have to be identified.

Table 1: Typical parameters to identify with the use of Chaboche model

Parameters	**Unit**	**Description**
E, ν	MPa, dimensionless	Young´s modulus, Poisson ratio
k	MPa	True elastic limit
Q_j, b_j	MPa, dimensionless	Non-linear isotropic hardening (N or N-1 times)
R_0	MPa	Linear isotropic hardening (0 or 1 time)
C_i, γ_i	MPa, dimensionless	Kinematic hardening (M times)
Z, n	MPa, dimensionless	Viscosity

3 Experimental data

3.1 Defined tests

The identification of the Young´s modulus and the determination of the parameters defining the kinematic hardening and isotropic hardening of the material are based on stress-strain measurements from uniaxial low cycle fatigue tests.
The determination of the true elastic limit and the viscosity parameters has been performed using time dependent stress measurements during uniaxial stress relaxation tests performed at high temperatures. A representative hold period has been considered for the stress relaxation tests.
In addition to the cyclic tests and the stress relaxation tests, uniaxial cyclic dwell tests with identical hold periods in tension and compression have been carried out at high temperatures to provide experimental data for the assessment of the accuracy of all defined parameters values.
The uniaxial low cycle fatigue tests were performed up to failure in strain-controlled mode with a fixed total strain range of 2 %, strain ratio of -1, and at strain rate of 0.2 %/s. A trapezoidal wave form was used as the load path.
The uniaxial stress relaxation tests have been performed at a strain level of 1% with a loading rate of 0.2 %/s. The strain has been hold at that level for a period of 600 s.
The uniaxial dwell tests have been performed in strain-controlled mode for a total strain range of 2 %, a strain ratio of -1, and a strain rate of 0.2 %/s. For every cycle, the strain has been holding at extreme values in tension and compression for a period of 600 s.
The strain amplitude value of 1 % and the hold period of 600 s are quite representative of the load conditions of a combustion chamber wall in service.

3.2 Test specimen

The test samples used for the different tests show the same geometry and dimensions. The shape and the dimensions of the rotatory-symmetric test specimens are illustrated in **Figure 1**.

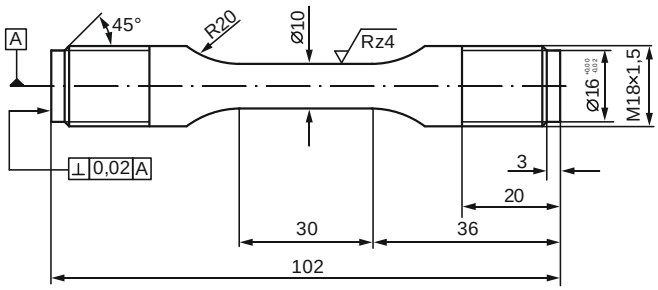

Figure 1: Drawing of the test specimen (geometry and dimensions)

3.3 Presented data

Although various temperatures have been defined for the characterization of the mechanical behaviour of the investigated cost efficient copper alloy, only the results related to the temperature of 900 K, at which the viscous behaviour of the material should be significant, are reported in the present paper to illustrate the step-by-step procedure adopted to identify the unified Chaboche constitutive model´s parameters of the tested copper alloy.

4 Identification of the parameters

The identification of the material constants is performed adopting a step-by-step procedure. Initial values of the parameters are estimated processing the experimental data. These initial values are then used in an optimization routine based on a nonlinear least square fit to get accurate and reliable optimized material parameters.
The estimation of the initial parameters requires representative, quality experimental data so that a given parameter may be estimated using the test results sensitive to that particular parameter.

4.1 Young´s modulus

The Young´s modulus E corresponds to the slope of the initial linear region of the stress-strain curve from a uniaxial monotonic tensile test. The plot of the first-quarter cycle of the first stress-strain hysteresis loop has been used as an alternative to a monotonic tensile test curve in the present work.

4.2 Isotropic hardening parameters

Experimental data from the low cycle fatigue test performed at 900 K show a rapid decrease of the stress range over the first few cycles followed with a steady decrease of the stress range when the number of cycles increases.

Assuming the change in the size of the yield surface is essentially isotropic, the evolution of the stress range with the number of cycles can be used to estimate the isotropic hardening parameters. To capture the particular evolution of the stress range with the number of cycles for the investigated copper alloy which has shown cyclic softening, the evolution of the isotropic hardening R associated with the contraction of the yield stress (present case) is defined as the sum of a non-linear isotropic hardening term R_1 (equation 12) and a linear isotropic hardening term R_2 (equation 13) as follows

$$\dot{R} = \dot{R_1} + \dot{R_2} = b(Q - R_1)\dot{p} + R_0\dot{p}$$
$$R_1 = 0 \text{ for } p = 0 \tag{16}$$

where Q is the stationary value of R_1 while b indicates the speed with which the stationary value is reached. R_0 is the asymptotic value of the isotropic variable R.
The evolution of the isotropic hardening R may be obtained by integrating equation 16 with respect to time as

$$R = R_1 + R_2 = Q(1 - e^{-bp}) + R_0 p \tag{17}$$

While R_1 describes the initial short-range transient isotropic hardening where Q is the stationary value of R_1 and b indicates the speed with which the stationary value is reached, R_2 is the asymptotic value of the isotropic variable R at large values of accumulated plastic strain p.
As the change in the size of the yield surface is assumed essentially isotropic, the evolution of the stress range with the number of cycles can be used to estimate R_0, Q and b.
The evolution of R is related to the change in stress range during the cyclic tests via

$$R \cong \frac{\Delta\sigma_i - \Delta\sigma_1}{2} \tag{18}$$

where $\Delta\sigma_1$ and $\Delta\sigma_i$ are the stress ranges for the first and ith cycles, respectively.

Defining $\Delta\varepsilon_p = \Delta\varepsilon - \Delta\sigma/E$ and assuming $p \approx 2N\Delta\varepsilon_p$ [1], the parameter R_0 is obtained as the slope in the regression of R vs. p for intermediate to large values of the accumulated plastic strain as shown in **Figure 2**. The deviation of R from the asymptotic behaviour at very large values of p is assumed to be the result of the accumulation of large damage in the material that later induced the failure of the sample. As this behaviour is assumed to be more related to material damage than the mechanical behaviour of the material, the corresponding data are not considered for the identification of the isotropic hardening parameters.

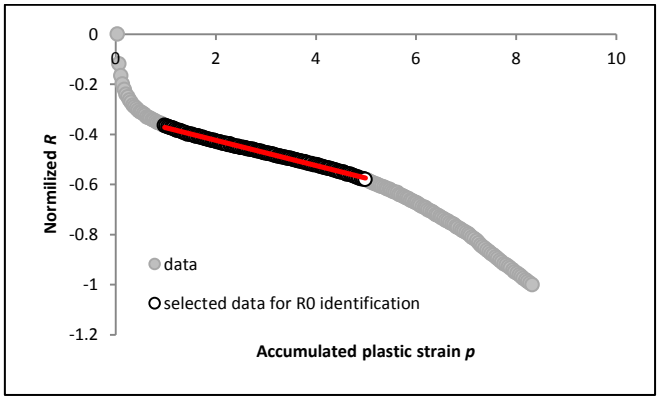

Figure 2: Plot used in the calculation of the asymptotic value R_0 of the isotropic hardening R

Considering the lower accumulated plastic strain region e.g. low values of p, and differentiating equation 17 with respect to p, rearranging and taking natural logs of both sides gives

$$\ln\left(R_0 - \frac{\partial R}{\partial p}\right) = -bp + \ln(-bQ) \tag{19}$$

For low values of p, the values of $\partial R/\partial p$ can be approximated by fitting the data (R, p) and differentiating the obtained equation of the fit relative to p. Therefore, plotting $\ln(R_0 - \partial R/\partial p)$ vs. p as shown in **Figure 3** allows the identification of b from the slope of the fit straight line, and Q from the y-axis intercept.

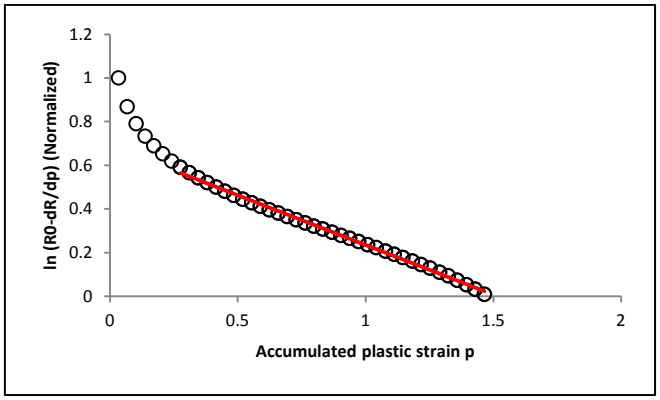

Figure 3: Plot used for the identification of the values Q and b for R_1

4.3 Kinematic hardening parameters

In the present paper, the kinematic hardening χ is defined as the sum of two terms

$$\chi = \sum_{i=1}^{2} \chi_i = \chi_1 + \chi_2 \tag{20}$$

The first part of the kinematic hardening χ_1 describes the transient region of the inelastic deformation, while the second part χ_2 describes the behaviour at greater inelastic deformations when χ_1 has reached the saturation value C_1/γ_1. For a given load as in tension-compression, these terms may be estimated by integrating equation (9) with respect to time as

$$\chi_i = \nu \frac{C_i}{\gamma_i} + \left(\chi_i^0 - \nu \frac{C_i}{\gamma_i}\right) \exp\left(-\nu\gamma_i\left(\varepsilon_p - \varepsilon_p^0\right)\right) \tag{21}$$

where $\nu = \mathrm{sgn}(\sigma - \chi) = \pm 1$ according to the direction of the viscoplastic flow, ε_p^0 and χ_i^0 correspond to the initial value, for example at the beginning of each plastic flow, of ε_p and χ_i, respectively.

Since the transformation of the yield surface following a monotonic loading is essentially kinematic, data from a monotonic test or from the first hysteresis loop of a cyclic test can be used to determine the kinematic parameters C_i and γ_i.

Substituting equation (17), (20) and (21) into equation (15) gives

$$\sigma = \sum_{i=1}^{2} \chi_i\left(\varepsilon_p, \chi_i^0, \varepsilon_p^0\right) + \nu \sum_{j=1}^{2} R_j(p) + \nu k + \nu\sigma_v \tag{22}$$

The stress and strain measurements from the first cycle of the uniaxial low cycle fatigue test are used for the identification of the kinematic hardening parameters C_1, γ_1, C_2, γ_2. As shown in **Figure 4**, data from two sections of the first hysteresis loop from the cyclic test are commonly used to get a first approximation of these parameters: data from the first tensile quarter cycle (section AB) [2] [6] [7] or data from the first tensile half cycle (section CD) [1] [8].

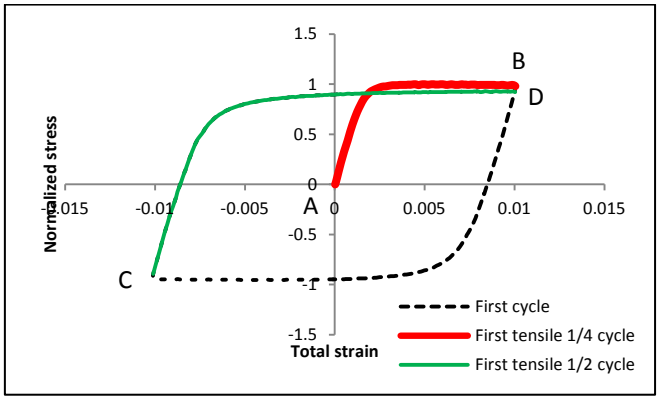

Figure 4: Plot of the first cycle from the uniaxial low cycle fatigue test showing the two sections commonly used to get a first approximation of the kinematic hardening parameters

Although the first tensile half cycle provides more data over a larger strain range for the approximation of the kinematic hardening parameters, the difficulty in assessing the initial values of the kinematic hardening χ_i^0 and χ_2^0 make the use of data from the first tensile quarter cycle more convenient and more reliable.

Indeed, if only data from the first quarter of the first stress-strain hysteresis loop are used, therefore $\sigma - \chi > 0$ with $\nu = \mathrm{sgn}(\sigma - \chi) = 1$, $p = \varepsilon_p$, $\varepsilon_p^0 = 0$, and $\chi_i^0 = 0$.

For the first tensile quarter cycle from the cyclic test, equation (21) is simplified to

$$\chi_i = \frac{C_i}{\gamma_i}\left(1 - \exp\left(-\gamma_i \varepsilon_p\right)\right) \tag{23}$$

Substituting equation (23) into equation (22) gives

$$\sigma = \sum_{i=1}^{2} \chi_i\left(\varepsilon_p\right) + \sum_{j=1}^{2} R_j(p) + k + \sigma_v \tag{24}$$

Considering the data from the first tensile quarter cycle from the cyclic test and if the later stages of hardening are considered, it can be assumed that χ_1 has reached the stationary value of C_1/γ_1 and therefore the hardening is dominated by χ_2. Consequently, equation (24) can be simplified to

$$\sigma = \frac{C_1}{\gamma_1} + \frac{C_2}{\gamma_2}\left(1 - \exp\left(-\gamma_2 \varepsilon_p\right)\right) + R + k + \sigma_v \tag{25}$$

Assuming k and σ_v as constant and differentiating equation (25) with respect to ε_p, rearranging and taking natural logs in both sides gives

$$\ln\left(\frac{\partial \sigma}{\partial \varepsilon_p} - \frac{\partial R}{\partial \varepsilon_p}\right) = -\gamma_2 \varepsilon_p + \ln(C_2) \tag{26}$$

The parameters γ_2 and C_2 may be obtained by the slope and the intersection, respectively, of the regression line through the data points in the $\ln(\partial\sigma/\partial\varepsilon_p - \partial R/\partial\varepsilon_p)$ vs. ε_p plot as illustrated in the following **Figure 5**.

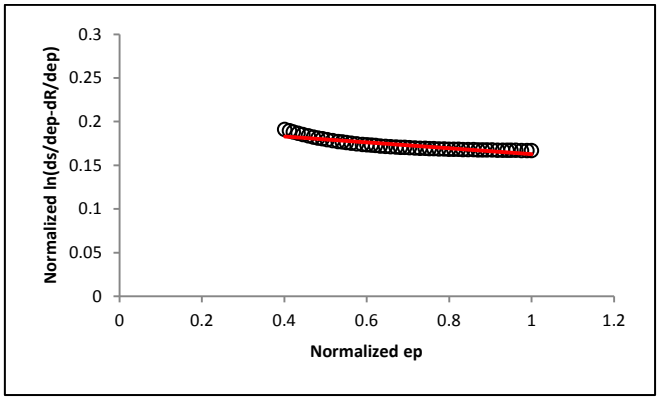

Figure 5: Plot used in the approximation of the parameters C_2 and γ_2 of the kinematic hardening χ_2

Similarly, if the early stages of hardening are considered, both χ_1 and χ_2 are contributing to the kinematic hardening. Since C_2 and γ_2 are known, the contribution of χ_2 into the hardening can be quantified.
Therefore, equation (24) can be rewritten as

$$\sigma = \frac{C_1}{\gamma_1}\left(1 - \exp\left(-\gamma_1 \varepsilon_p\right)\right) + \chi_2 + R + k + \sigma_v \tag{27}$$

Assuming k and σ_v as constant and differentiating equation (27) with respect to ε_p, rearranging and taking natural logs in both sides gives

$$\ln\left(\frac{\partial \sigma}{\partial \varepsilon_p} - \frac{\partial \chi_2}{\partial \varepsilon_p} - \frac{\partial R}{\partial \varepsilon_p}\right) = -\gamma_1 \varepsilon_p + \ln(C_1) \tag{28}$$

The parameters γ_1 and C_1 may be obtained by the slope and the intersection, respectively, of the regression line through the data points in the $\ln(\partial\sigma/\partial\varepsilon_p - \partial\chi_2/\partial\varepsilon_p - \partial R/\partial\varepsilon_p)$ vs. ε_p plot as illustrated below in **Figure 6**.

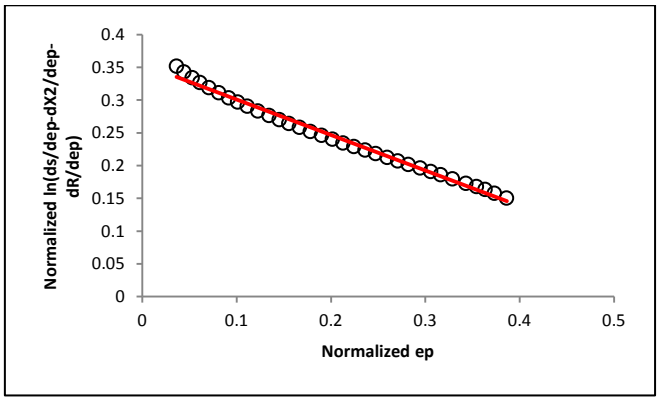

Figure 6: Plot used in the approximation of the parameters C_1 and γ_1 of the kinematic hardening χ_1

As shown in equation (26) and (28), the expressions of $\partial\sigma/\partial\varepsilon_p$ and $\partial R/\partial\varepsilon_p$ have to be defined in order to obtain the data points used for the fit.

As $p = \varepsilon_p$ for the first quarter cycle of the first cycle, the expression of $\partial R/\partial\varepsilon_p$ can be obtained by differentiating equation (17) relative to ε_p

$$\frac{\partial R}{\partial \varepsilon_p} = R_0 + Qb\exp\left(-b\varepsilon_p\right) \tag{29}$$

The definition of the expression of $\partial\sigma/\partial\varepsilon_\mathrm{p}$ is not as straightforward as for $\partial R/\partial\varepsilon_p$. A procedure for the definition of the expression of $\partial\sigma/\partial\varepsilon_\mathrm{p}$ is given in [2]. Starting from the term $\mathrm{d}\sigma/\mathrm{d}\varepsilon_p$, multiplying by $\mathrm{d}t/\mathrm{d}t$ and $\mathrm{d}\varepsilon_t/\mathrm{d}\varepsilon_t$, then rearranging results in

$$\frac{d\sigma}{d\varepsilon_p} = \frac{d\sigma}{d\varepsilon_t}\frac{1}{\dot{\varepsilon_p}}\dot{\varepsilon}_t \tag{30}$$

Since the tests are strain controlled, the value of the total strain rate $\dot{\varepsilon}_t$ is known.
Defining the total strain ε_t as the sum of its elastic part ε_e and its plastic part ε_p, and using the Hook´s law, $\varepsilon_e = \sigma/E$ result in

$$\varepsilon_t = \frac{\sigma}{E} + \varepsilon_p \tag{31}$$

Rearranging equation (31) and differentiating it with respect to time gives

$$\frac{d\varepsilon_p}{dt} = \frac{d\varepsilon_t}{dt} - \frac{1}{E}\frac{d\sigma}{dt} \tag{32}$$

Multiplying the final term in equation (32) by $\mathrm{d}\varepsilon_t/\mathrm{d}\varepsilon_t$ and rearranging leads to

$$\dot{\varepsilon_p} = \dot{\varepsilon}_t\left(1 - \frac{1}{E}\frac{d\sigma}{d\varepsilon_t}\right) \tag{33}$$

An expression of $\mathrm{d}\sigma/\mathrm{d}\varepsilon_t$ is required in equation (33) to define $\dot{\varepsilon_p}$ and also in equation (30) for the calculation of $\mathrm{d}\sigma/\mathrm{d}\varepsilon_p$.

The Ramberg-Osgood equation can be used to describe the evolution of σ as a function of ε_t along the tensile portions of the stress-strain hysteresis loop. To describe the first tensile quarter cycle of the first cycle (section AB in **Figure 4**), the Ramberg-Osgood equation is expressed in the following form

$$\varepsilon_t = \frac{\sigma}{E} + \frac{\sigma_0}{E}\left(\frac{\sigma}{\sigma_0}\right)^{n_0} \tag{34}$$

where σ_0 and n_0 are the parameters of the Ramberg-Osgood equation.

Differentiating equation (34) with respect to ε_t gives

$$\frac{d\sigma}{d\varepsilon_t} = \frac{E}{1 + n_0\left(\frac{\sigma}{\sigma_0}\right)^{n_0-1}} \tag{35}$$

Rearranging equation (35) and taking logs of both sides gives

$$\ln(E\varepsilon_t - \sigma) = n_0\ln(\sigma) - (n_0 - 1)\ln(\sigma_0) \tag{36}$$

The parameters n_0 and σ_0 may be obtained by the slope and the intersection, respectively, of the regression line through the data points in the $\ln(E\varepsilon_t\text{-}\sigma)$ vs. $\ln(\sigma)$ plot as show in **Figure 7**.

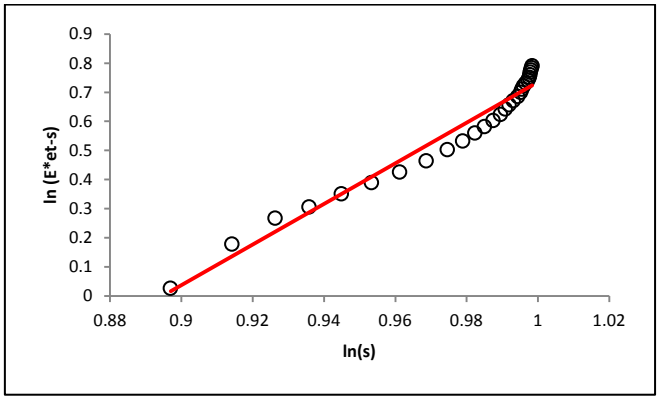

Figure 7: Plot used in the calculation of the constants n_0 and σ_0 of the Ramberg-Osgood equation

4.4 Viscous parameters

The rate dependency of the stress and therefore the creep effect is accounted for within the model in the form of the Norton creep law. Considering uniaxial stress relaxation tests, where $p = \varepsilon_p$ and $v = sgn(\sigma - \chi) = 1$, and substituting equation (14) into equation (15), the viscous stress can be defined as

$$Z\dot{\varepsilon_p}^{1/n} = \sigma_v = \sigma - \chi - R - k \tag{37}$$

At the beginning of the stress relaxation test, $\varepsilon_p^0 = 0$ and $\chi_i^0 = 0$. Therefore, the kinematic hardening χ_i is defined using equation (23).
As the parameters for the isotropic hardening and the kinematic hardening are known, the contributions of χ and R can be quantified. A first estimation of the true elastic limit k is obtained by observing that $\sigma_v = 0$ for $t \rightarrow \infty$. As shown in **Figure 8**, the value of $\sigma - \chi - R$ after 600 s of stress relaxation can then be regarded as an upper bound for k (the lower bound obviously being $k_{min} = 0$).

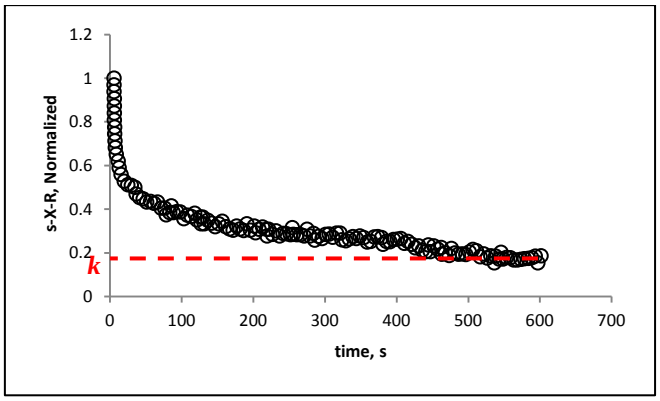

Figure 8: Plot used for a first estimation of the true elastic limit k

Considering a stress relaxation test, in which $\dot{\varepsilon} = 0$, so at constant temperature ($\dot{\varepsilon}_{th} = 0$), the plastic strain increment $\dot{\varepsilon}_p$ is defined from equation (1) as

$$\dot{\varepsilon} = 0 = \dot{\varepsilon}_e + \dot{\varepsilon}_{th} + \dot{\varepsilon}_p = \frac{\dot{\sigma}}{E} + \dot{\varepsilon}_p \Rightarrow \dot{\varepsilon}_p = -\frac{\dot{\sigma}}{E} \tag{38}$$

Approximating the stress increment $\dot{\sigma}$ using centred finite difference, instantaneous values for the plastic strain rate can be obtained using equation (38).
As the value of k is determined, and as σ, χ, and R are known for all the data points obtained from the stress relaxation test, the viscous stress σ_v can be calculated using equation (37).
Rearranging equation (37) and taking logs of both sides gives

$$\ln(\sigma_v) = \frac{1}{n}\ln\left(\dot{\varepsilon}_p\right) + \ln(Z) \tag{39}$$

The parameters n and Z can be determined by plotting the viscous stress σ_v against $\dot{\varepsilon}_p$ in a log-log plot as shown in **Figure 9**.

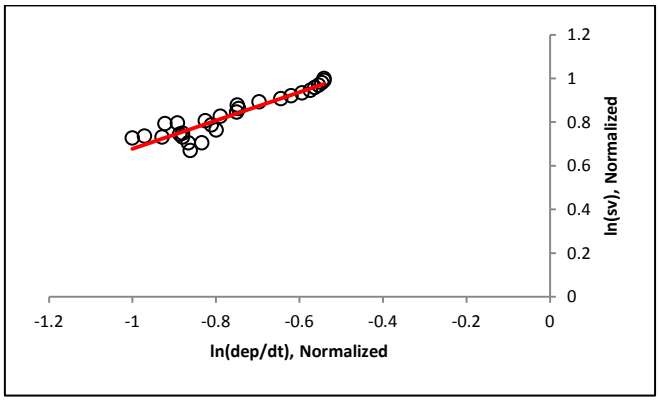

Figure 9: Plot used in the calculation of the constants n and Z of the Norton creep law

5 Accuracy of the identified model´s parameters

5.1 Optimization procedure

The model parameters are identified using a step by step procedure. The initial parameters estimated were used as inputs in the optimization procedure. The objective function as defined by equation (40) was used to quantify the difference between the experimental stress values and the corresponding calculated stress values with a given set of parameters. The goal is to determine a set of parameters that minimizes the objective function

$$F(x_n) = \frac{1}{Y}\sum_{r=1}^{Y}\left(\sigma_r^{num}(x_n) - \sigma_r^{exp}\right)^2 \tag{40}$$

where σ^{num} and σ^{exp} denote numerical analysis results and experimental measurements; x_n represents the set of parameters and Y is the number of data points in the experiment.

The optimization of the kinematic hardening coefficients using equation (24) for the calculation of σ^{num} and the data from the first quarter cycle of the first cycle of the fatigue test as σ^{exp} resulted in a poor prediction of the hysteresis loops with rapid hardening [8]. In the present work, equation (22) is used for the calculation of σ^{num} and the experimental data from both the first compression half cycle (section BC in **Figure 4**) and the first tensile half cycle (section CD in **Figure 4**) of the first cycle from the low cycle fatigue test are considered for the optimization of the kinematic hardening coefficients.

The gradient-based Levenberg-Marquardt iteration algorithm has been used to determine the optimum set of material parameters by solving the nonlinear least squares fit problem given by equation (40). For this purpose, the Optimization Toolbox of MATLAB, and more specifically the “lsqcurvefit” command was applied.

5.2 Implementation of Chaboche model in MATLAB

A first-order non-linear system of differential equations can be obtained from equations (2) to (13) with considering the variables of σ, χ_1, χ_2, R_1, R_2, ε_p, and p. The solution of the Chaboche model is obtained by using the optimized parameters and by solving the above mentioned system of differential equations using the automatic adaptive variable step Runge-Kutta-Fehlberg algorithm, one of the most popular methods of solving differential equations using numerical techniques.
The ODE45 function within the MATLAB mathematics toolbox, in which the variable step length Runge-Kutta-Fehlberg algorithm is used, has been used for solving the first-order system of differential equations from the initial values problem.

5.3 Comparison of the model results to experimental data

The solution of the numerical model using the optimized material parameters is compared with the experimental data from uniaxial strain-controlled low cycle fatigue test and dwell test with 600 s hold periods in tension and compression at 900K to assess the accuracy of the determined model´s coefficients.

5.3.1 Hysteresis loops

The numerical analysis of a cyclic test that would be performed in strain-controlled mode with a fixed total strain range of 2 %, a strain ratio of -1, and at a strain rate of 0.2 %/s for the cycle 1, 5, and 40 is compared to the corresponding hysteresis loops from the uniaxial low cycle fatigue test performed at the same conditions in **Figure 10**. As for the uniaxial low cycle fatigue test, a trapezoidal wave form was used as load path for simulating the uniaxial cyclic test. Globally, the shapes of the numerical and experimental stress-strain curves coincide well. A good correlation between the simulation and the experimental data was obtained over the whole strain range and for all cycles.

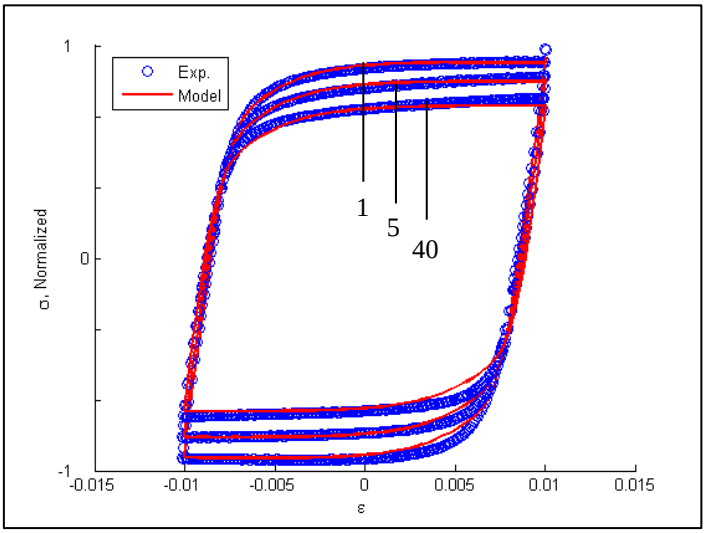

Figure 10: Comparison of the model prediction of the 1st, 5th, and 40th cycle to the corresponding hysteresis loops from the strain-controlled LCF test performed at 900 K.

5.3.2 Evolution of the stress amplitude with the cycle number

Figure 11 compares the evolution of the stress range with the accumulated plastic strain from the uniaxial low cycle fatigue test to the cyclic softening of the material predicted by the model considering the same conditions. The numerical results show a good agreement with the measurement since the two representative curves almost overlap. The two stages of the cyclic softening are well predicted by the model.

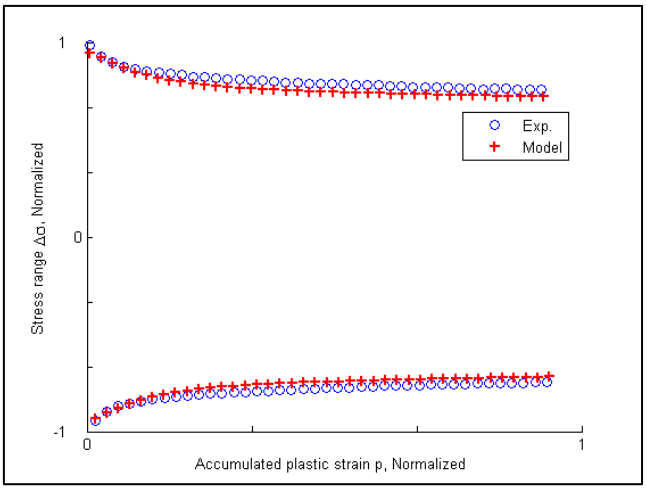

Figure 11: Comparison of the model prediction of the cyclic softening of the material to the evolution of the stress range during the considered strain-controlled LCF test performed at 900 K.

5.3.3 Dwell test with 600 s hold periods in tension and compression

In addition to the cyclic tests and the stress relaxation tests, uniaxial cyclic dwell tests with identical hold periods in tension and compression have been carried out at high temperatures to provide experimental data for the assessment of the accuracy of all defined parameter values.
The uniaxial dwell tests have been performed in strain-controlled mode for a total strain range of 2 %, a strain ratio of -1, and a strain rate of 0.2 %/s. For each cycle, the strain was hold at extreme values in tension and compression for periods of 600 s.
In **Figure 12**, the stress evolution with time predicted by the numerical model is compared to the measurement of the stress during the dwell test performed at 900 K. The numerical model slightly overestimates the stress range before the hold periods. However, the reduction of the stress range with increasing time is well simulated by the model as the difference between the predicted stress range and the measured one is constant for all the cycles. As far as creep is concerned, the model predicts a bit faster relaxation of the stress compared to the experiment. Globally, the correlation between the model prediction and the measured stress evolution is acceptable.

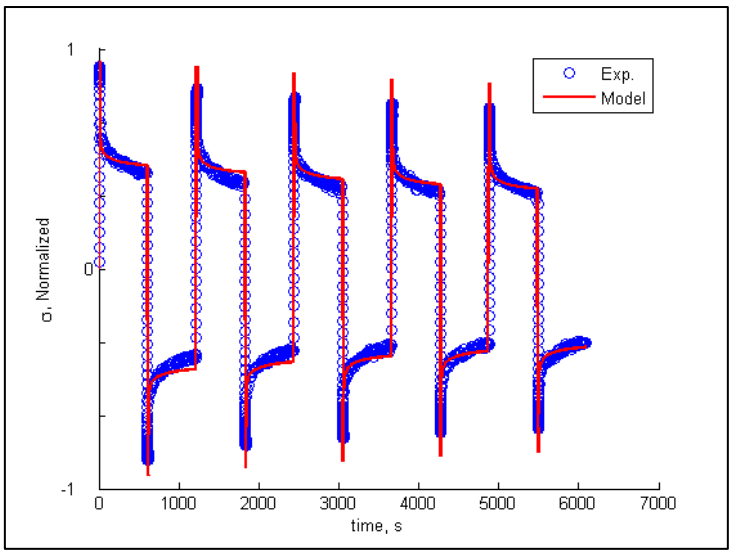

Figure 12: Comparison of the stress evolution with time predicted by the model for the simulation of a dwell test with 600 s hold periods in tension and compression to the experience at 900 K

6 Conclusion

Driven by the intention to increase the fatigue life of rocket engines while reducing its cost, a cost effective copper based alloy has been investigated. The unified Chaboche model was selected for the simulation of the mechanical behaviour of this material.
Strain-controlled uniaxial low cycle fatigue tests and stress-relaxation tests have been used for the determination of the model´s parameters. The considered step by step procedure to estimate initial values of the model´s parameters has been presented. The used equations and considered experimental data have been shown in detail.
The above mentioned estimated initial parameters were used as input values for the non-linear least squares fit procedure based on the Levenberg-Marquardt iteration algorithm. The constitutive equations of the Chaboche model have been implemented in MATLAB to assess the accuracy of the fitted parameters. The predictions of the model using the optimized parameters show a good agreement with the experimental data for the considered uniaxial tests. Therefore, the values of the model´s parameters can be assumed as accurate.

References

[1] J. Tong, Z. L. Zhan and B. Vermeulen, "Modelling of cyclic plasticity and viscoplasticity of a nickel-based alloy using Chaboche constitutive equations", *International Journal of Fatigue 26*, pp. 829-837, 2004.

[2] Y. P. Gong, C. J. Hyde, W. Sun and T. H. Hyde, "Determination of material properties in the Chaboche unified viscoplasticity model", *Proc. IMechE Vol. 224 Part L: J. Materials: Design and Application*, pp. 19-29, 2009.

[3] J. Chaboche and G. Rousselier, "On the plastic and viscoplastic constitutive equations (Part I and II)", *Journal of Pressure Vessel Technology 105*, pp. 153-159, 1983.

[4] P. J. Amstrong and C. O. Fredericks, "A mathematical representation of the uniaxial Bauschinger effect", CEGB Report RD/B/N731, 1966.

[5] F. H. Norton, The creep of steel at high temperature, New York: McGraw Hill, 1929.

[6] J. Tong and B. Vermeulen, "The description of cyclic plasticity and viscoplasticity of waspaloy using unified constitutive equations", *International Journal of Fatigue*, pp. 413-420, 2003.

[7] L. G. Zhao, J. Tong, B. Vermeulen and J. Byrne, "On the uniaxal mechanical behaviour of an advanced nickel base superalloy at high temperature", *Mechanics of Materials 33*, pp. 593-600, 2001.

[8] W. Bouajila and J. Riccius, "Identification of the unified Chaboche constitutive model´s parameters for a cost efficient copper-based alloy", in *Space Propulsion*, Cologne, 2014.